Journal of Sound and Vibration (2002) **254**(1), 117–141
doi:10.1006/jsvi.2001.4089, available online at http://www.idealibrary.com on IDEAL®

FEEDFORWARD ADAPTIVE CONTROL OF FLEXURAL VIBRATION IN A BEAM USING WAVE AMPLITUDES

C. R. HALKYARD

Department of Mechanical Engineering, University of Auckland, Private Bag 92019, *Auckland, New Zealand. E-mail: r.halkyard@auckland.ac.nz*

AND

B. R. MACE

*Institute of Sound and Vibration Research, University of Southampton, Highfield, Southampton SO*17 1*BJ, England*

(*Received* 5 *February* 2001, *and in final form* 4 *October* 2001)

This paper concerns the real-time estimation of wave amplitudes and their subsequent use as a cost function in adaptive active control of bending vibrations in a beam. The amplitude of the wave propagating downstream from the control location is estimated by filtering the outputs of an array of sensors. Minimizing this wave amplitude has significant advantages over the more conventional approach in which velocity at some point is minimized. Expressions for the ideal frequency responses of the wave filters are found for the case of an array comprising two sensors in the far field. These filters are non-causal. FIR implementations designed using direct and time-delay methods are described, the latter offering some substantial advantages. Practical performance considerations are discussed, including filter length, frequency range, effects of near fields, group delays, accuracy and cross-sensitivity. Simulations and experimental measurements are performed and compared.
© 2002 Elsevier Science Ltd. All rights reserved.

1. INTRODUCTION

The use of an appropriate cost function in an adaptive control system can be critical to the system performance. Naturally, the choice of cost function depends strongly on the overall objective of the control. If control of vibration at a point is desired, then the vibration level at that point is an obvious cost function, and this approach has been used in many studies (e.g., references [1–4]). However, minimizing vibration at a point does not guarantee low *overall* vibration levels in a structure. For a better *global* performance, it may therefore be preferable to use an alternative cost function, with one possibility being propagating wave amplitude. In particular, one might choose to minimize the amplitude of the outward-propagating wave downstream of the control location. This type of control forms the subject of this paper.

A wave propagation model has been used in active vibration control by a number of researchers (e.g., references [5–9]). To use wave amplitude as a cost function, however, it is first necessary to obtain real-time estimates of the required wave amplitude, and this has been considered in a number of studies (e.g., references [10–12]). In this paper, the wave amplitude estimates will be derived by digitally filtering, and combining, the outputs obtained from an array of sensors. A systematic design method for the digital filters was presented in reference [13] with real-time intensity measurement applications in mind: this

0022-460X/02/$35.00 © 2002 Elsevier Science Ltd. All rights reserved.

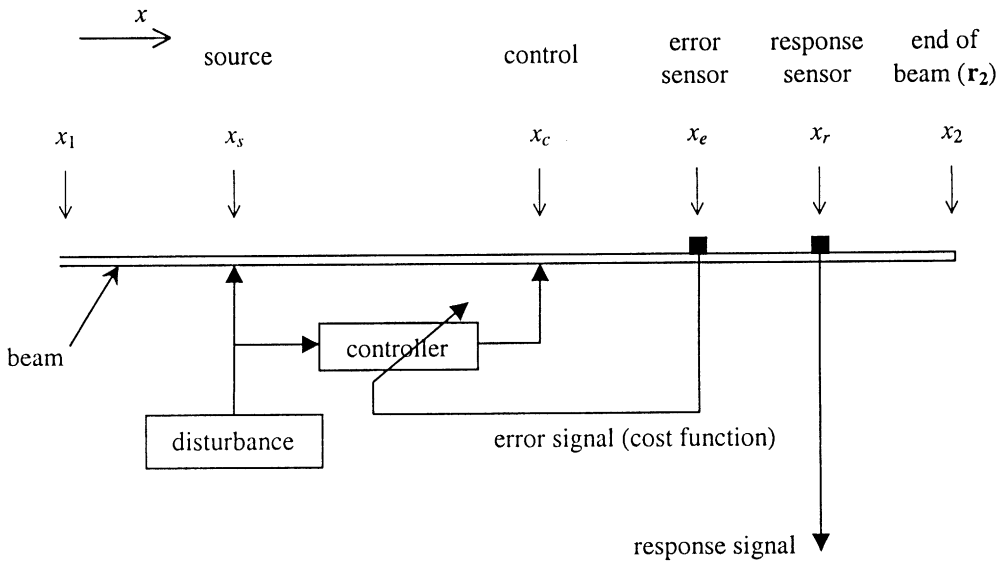

Figure 1. Feedforward control of bending vibrations.

approach will be described further in this paper. Specifically, this paper describes the application of wave-based adaptive control of vibrational energy flow to flexural vibration in beams, using a filtered-X LMS algorithm [14]. The following section describes the system being controlled, and this is followed by a description of the system behaviour in terms of waves. Next, the real-time estimation of wave amplitudes is discussed together with various performance considerations. Finally, the system is simulated numerically and implemented experimentally, and the results compared and discussed.

2. THE SYSTEM

In this paper, feedforward adaptive active control of flexural vibration in a beam is considered. A schematic diagram of the system is shown in Figure 1. A disturbance is produced by some source, and excites vibrations of the beam by injecting waves at some point $x = x_s$. These waves travel through the structure producing unwanted vibrations in some remote region. A reference signal from this disturbance is assumed to be available, and this is the input to the digital controller, which produces a cancellation signal. This cancellation signal is used to excite additional controlling vibrations by injecting further waves at $x = x_c$.

The resulting vibration field comprises waves, excited by both the disturbance and the control, which travel in both directions along the beam. In general, waves will be reflected from the ends of the beam. In one limiting case, where the amplitudes of these reflections are negligible, the beam appears to be infinitely long. In a finite beam, however, the reflections lead to resonant behaviour of the beam and the wave field becomes a superposition of the travelling and standing waves. This can cause deterioration in the performance of the active control system.

The error sensor in Figure 1 provides an error signal that gives some measure of the resulting vibrations. In this paper, an error sensor is defined in a general way: the error sensor is some array of one or more response sensors such as accelerometers, strain gauges,

piezoelectric patches, etc.; these response sensors may measure point responses or may be distributed; the outputs of the response sensors may also be combined and filtered, using either analogue or digital filters or both, and the resulting output signal is defined as being the error signal. The error signal is used to perform two functions. The first is to quantify the control achieved, while the second is to provide a cost function that may be used to adaptively change the controller parameters to improve performance. In the simulations and experiments described, a filtered-X LMS algorithm is used for adaptation, but other adaptive algorithms may also be used.

One common approach to error sensing is to measure the resulting acceleration (or velocity) at the error location. The particular interest in this paper, however, is in obtaining and using an error signal that is proportional to the amplitude of the positive-going wave, rather than point velocity or acceleration. The theoretical benefits of using such an error signal, as opposed to a conventional point measurement, are shown in the following section.

3. STRUCTURAL DYNAMIC VARIABLES AND ERROR SENSORS

3.1. THE SYSTEM AND WAVES

The behaviour of the beam may be written in terms of propagating and nearfield wave amplitudes. These waves may be defined in terms of any dynamic variable, such as displacement or strain, but in this paper they will be defined in terms of velocity. In the region of the sensor array, the velocity of the beam is given in terms of these velocity wave components by

$$V(x, \omega) = \Phi_V^+(\omega)\mathrm{e}^{-\mathrm{i}kx} + \Phi_{N,V}^+(\omega)\mathrm{e}^{-kx} + \Phi_V^-(\omega)\mathrm{e}^{\mathrm{i}kx}, \tag{1}$$

where Φ_V^+ and Φ_V^- are the amplitudes of the propagating waves and $\Phi_{N,V}^+$ is the residual near field produced by the control. It is assumed that the amplitude of the upstream-going near field $\Phi_{N,V}^- \exp(kx)$ is negligible: this wave would typically be produced by reflections from the end at $x = x_2$, and the stipulation that $k(x_2 - x_e) \geqslant \pi$ will generally be sufficient to justify this assumption. In equation (1), k is the wavenumber, where

$$k = \alpha\sqrt{\omega}, \quad \alpha = \sqrt[4]{\sigma/EI} \tag{2}$$

with EI being the flexural stiffness of the beam and σ its mass per unit length. (A list of symbols is given in Appendix A.) In the presence of damping, k has a (usually small) negative imaginary part so that the amplitude of a propagating wave component decays gradually in the direction of propagation. The damping can therefore be characterized by

$$\varepsilon = -\frac{\mathrm{Im}(k)}{\mathrm{Re}(k)} \Rightarrow k = \mathrm{Re}(k)(1 - \mathrm{i}\varepsilon). \tag{3}$$

In this paper, it will be assumed that the decay of the propagating wave amplitude is negligible over distances of the order of the sensor separation. The near field of the disturbance is assumed to be negligible, while that of the control is included since the control may be applied close to the sensor array and this may adversely affect the performance of the system. The downstream propagating wave,

$$\Phi_V^+ = \Phi_{V,D}^+ + \Phi_{V,C}^+, \tag{4}$$

is the superposition of components from the disturbance and control. These may be considered as arising from the reference signal being filtered by the primary and secondary paths respectively.

The upstream propagating wave,

$$\Phi_V^- = \Phi_{V,0}^- + r\Phi_V^+; \quad r = R\mathrm{e}^{-\mathrm{i}\theta_r}, \tag{5}$$

also has two components. The first, $\Phi_{V,0}^-$, is produced by any additional vibration sources that may happen to act downstream (i.e., at $x > 0$), Φ_V^+ and $\Phi_{V,0}^-$ being incoherent. (Henceforth, it will be assumed that this component is negligible unless otherwise stated.) The second component, $r\Phi_V^+$, arises from the coherent reflection of Φ_V^+ from downstream boundaries or attachments. The reflection coefficient r is complex, its magnitude R being $\leqslant 1$ and its phase $(-\theta_r)$ is typically negative and decreases monotonically.

The performance of the control system will depend on the nature of the wave field that is present and on the cost function used. Two possible cost functions are considered in the following subsection: velocity and downstream-going propagating wave amplitude.

3.2. STRUCTURAL DYNAMIC VARIABLES AS COST FUNCTIONS

3.2.1. *Velocity as a cost function*

Consider the case of a single velocity sensor mounted at $x = 0$. If the output of this sensor is used as a cost function, then an ideal controller will force the velocity at the point to be zero. From equation (1), it follows that

$$\Phi_V^+ + \Phi_{N,V}^+ + \Phi_V^- = 0. \tag{6}$$

Since $\Phi_V^- = r\Phi_V^+$, then

$$\Phi_V^+ = -\frac{1}{1+r}\,\Phi_{N,V}^+ \tag{7}$$

and hence the required control is

$$\Phi_{V,C}^+ = -\frac{1}{1+r}\,\Phi_{N,V}^+ - \Phi_{V,D}^+. \tag{8}$$

A distance x further downstream the velocity will be

$$V(x,\omega) = -\frac{1}{1+r}\,\Phi_{N,V}^+(\omega)(\mathrm{e}^{-\mathrm{i}kx} + r\mathrm{e}^{\mathrm{i}kx}) + \Phi_{N,V}^+(\omega)\mathrm{e}^{-kx}. \tag{9}$$

Three points should be noted. Firstly, the near field deteriorates the performance, giving rise to some residual response away from the error sensor location. If a compact control system is required (i.e., the error sensor and control are close), then this could be substantial. Secondly, global control is not achieved, although the residual downstream vibrations would be small if the near field at the error sensor location $\Phi_{N,V}^+$ and R are small. Finally, reflections can cause substantial problems at certain frequencies, especially if $R \approx 1$. In effect, the residual near field is multiplied by the factor $1/(1+r)$, which can become very large if θ_r is an odd multiple of π. This is particularly true for lightly damped, finite structures, which are often the target for control. At these frequencies, the sensor is mounted at, or close to, a node of a standing wave originating at the boundary. The frequencies can be dense, since $\theta_r \sim 2kl_b$, where l_b is the distance to the boundary, which may be large. The

frequencies are also typically difficult to predict accurately, since they are sensitive to changes or uncertainties in the system properties such as the boundary conditions (e.g., changes in orientation, payload, etc.). It would, therefore, be difficult to compensate for the term $1/(1 + r)$ in a robust manner.

3.2.2. *Wave amplitude as a cost function*

If the positive-going wave amplitude Φ_V^+ is sensed and used as a cost function, the control adapts so that Φ_V^+ is zero. The residual velocity for $x \geqslant 0$ is then

$$V(x, \omega) = \Phi_{N,V}^+(\omega)\mathrm{e}^{-kx}, \tag{10}$$

and comprises solely the near field of the control. Thus, there is some localized response, but global control is achieved and the effects of downstream reflections are irrelevant. The required control effort is

$$\Phi_{V,C}^+ = -\Phi_{V,D}^+ \tag{11}$$

so that the control merely involves cancellation of the propagating wave. It is, therefore, apparent that there may be significant benefits in using wave amplitude as a cost function. However, conventional sensors measure the effects of the superposition of all wave components. In order to estimate the amplitude of an individual wave component, it is necessary to filter and combine the outputs of a number of sensors. This is discussed in the following sect.

4. WAVE AMPLITUDE ESTIMATION

In this paper, the error sensor is considered to be an array of response sensors, whose outputs are filtered and combined to yield an estimate of the required cost function. This section concerns how the outputs from two velocity sensors can be filtered to provide estimates of the positive-going velocity wave amplitude. Velocities are used for numerical convenience in this case, and in practice, accelerations would often be measured with velocities found by integration. The physical arrangement of the sensors is shown in Figure 2, where the co-ordinate x is now centered on the error sensor array. The velocity sensors are separated by a distance Δ, the control force is applied at $x = -l$, and the disturbance applied further in the negative direction, $-x$.

All filtering is performed digitally, with the velocities assumed to be sampled at a sampling frequency f_s, after being first passed through low-pass analogue anti-aliasing filters with a cut-off frequency of somewhat less than the Nyquist frequency $f_n = f_s/2$. The ideal frequency responses of the wave filters are defined at discrete, equally spaced frequencies, the aim being to design an FIR filter in the frequency domain which best

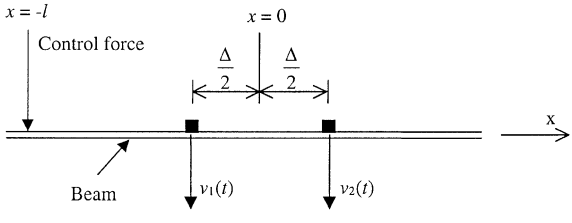

Figure 2. Error sensor array comprising two velocity sensors.

approximates the ideal filter (in a least-squares sense) and to implement it in the time domain. The filter is designed assuming that the near field $\Phi^+_{N,V}(\omega)$ is zero. This near field is included in the simulations, however.

Referring to equation (1), it is apparent that, under farfield conditions (i.e., $\Phi^+_{N,V} = 0$), the outputs of the velocity sensors are related to the wave amplitudes by

$$\begin{pmatrix} V_1 \\ V_2 \end{pmatrix} = \begin{bmatrix} e^{ik\Delta/2} & e^{-ik\Delta/2} \\ e^{-ik\Delta/2} & e^{ik\Delta/2} \end{bmatrix} \begin{pmatrix} \Phi^+_V \\ \Phi^-_V \end{pmatrix}. \tag{12}$$

Inverting this to solve for the wave amplitudes gives

$$\begin{aligned} \Phi^+_V &= H_1(\omega)(V_1(\omega) + V_2(\omega)) - H_2(\omega)(V_1(\omega) - V_2(\omega)), \\ \Phi^-_V &= H_1(\omega)(V_1(\omega) + V_2(\omega)) + H_2(\omega)(V_1(\omega) - V_2(\omega)), \end{aligned} \tag{13}$$

where

$$H_1 = \frac{1}{4\cos(k\Delta/2)}; \qquad H_2 = \frac{i}{4\sin(k\Delta/2)}. \tag{14}$$

Thus, by combining the outputs of the velocity sensors and filtering with filters having frequency responses $H_1(\omega)$ and $H_2(\omega)$, the amplitudes of the two waves may be determined. It should be noted that these expressions also apply to acoustic waves in a duct, as described by Swinbanks [10], except that here, of course, the waves are dispersive.

In what follows, frequencies will be normalized with respect to the sampling frequency so that the Nyquist frequency corresponds to $\omega = \pi$. Distances will be normalized with respect to the wavelength λ_n at the Nyquist frequency, and hence $k = (2\sqrt{\pi}/\lambda_n)\sqrt{\omega}$.

4.1. FREQUENCY RANGE AND SENSOR ARRAY DIMENSIONS

Control is to be applied over a frequency range from ω_{min} to ω_{max}. There are a variety of influences on these limiting frequencies, one of which is filter accuracy. The filters are accurate over a frequency range that is limited by a number of factors. The first of these is the cut-off frequency of the anti-aliasing filters and the sampling frequency, the maximum frequency of control being less than the Nyquist frequency. Secondly, H_1 becomes infinite if $k\Delta = \pi$. This imposes a maximum separation for a given frequency range so that $\Delta/\lambda_n < 0{\cdot}5$. Thirdly, a lower frequency limit ω_{min} is imposed by the requirement that the array should (in principle) be free from the influence of the near field of the control so that, from Figure 2, $\exp(-k(l - \Delta/2)) \ll 1$. For example, if the sensor is always to be at least half a wavelength from the control, then the maximum contribution of the near field to the sensor outputs is $\exp(-\pi) \approx 0{\cdot}04$. The lower frequency limit and the array location are then related by

$$2\sqrt{\frac{\omega_{min}}{\pi}}\left(l - \frac{\Delta}{2}\right) = 1. \tag{15}$$

4.2. FIR FILTER DESIGN

The ideal impulse responses $h_1(t)$ and $h_2(t)$ of the digital filters can, in principle, be found from the inverse Fourier transforms of $H_1(\omega)$ and $H_2(\omega)$. However, these impulse responses are non-causal, which causes some problems in practical implementation. In this section,

two methods for the design of the FIR filters are described and some numerical results are presented.

4.2.1. *Direct method*

The first method of filter design is to use a least-squares approach in the frequency domain. However, since the ideal filters are non-causal, the result is a filter whose frequency response approximates this ideal. The filter output at each time step gives an estimate of the wave amplitude at that time. In the examples shown, these digital filters were designed in Matlab® using the function *invfreqz*.

4.2.2. "*Time-delay*" *method*

In the time-delay approach, an $n_t = (2n_d + 1)$ term filter is designed by time-delaying the filters H by n_d time steps. This involves multiplying the ideal frequency response by $\exp(-\mathrm{i}\omega n_d)$. A filter is then designed using the same least-squares procedure. The output of the filter at each time step is an estimate of the wave amplitude n_d time steps before. These filters are substantially more accurate, but introduce time delays of n_d steps, which affect the maximum adaptation rate, but only very modestly.

4.3. COMPARISON OF FILTER DESIGN METHODS

The performances of the implemented filters may be compared both in terms of their accuracy and cross-sensitivity, which relate the filter output to the actual amplitudes of the positive- and negative-going waves. They are defined by

$$\frac{|\hat{\Phi}_V^+|^2}{|\Phi_V^+|^2} = 4\left|\hat{H}_1 \cos\left(\frac{k\Delta}{2}\right) - \mathrm{i}\hat{H}_2 \sin\left(\frac{k\Delta}{2}\right)\right|^2,$$

$$\frac{|\hat{\Phi}_V^+|^2}{|\Phi_V^-|^2} = 4\left|\hat{H}_1 \cos\left(\frac{k\Delta}{2}\right) + \mathrm{i}\hat{H}_2 \sin\left(\frac{k\Delta}{2}\right)\right|^2, \tag{16}$$

where $\hat{\Phi}_V^+$ is the estimated value of the positive-going wave and $\hat{H}_1$ and $\hat{H}_2$ are the frequency responses of the implemented filters. Ideally, the accuracy should have a value of unity, while the cross-sensitivity should be zero. All comparisons depend on the sensor spacing and the number of terms in the filter. Numerical results are, therefore, presented for filters of moderate order, and for sensors having a typical spacing.

Figures 3 and 4 show the characteristics and performance of FIR filters with $n_t = 7$ terms, the sensor separation being $\Delta = 0{\cdot}3\lambda_n$. Figures 5 and 6 show similar results for significantly longer filters with $n_t = 21$ terms. It is apparent that filters designed using the time-delay approach are significantly more accurate, with exact phases, and are much less sensitive to negative-going waves than those designed using the direct approach. The bandwidths of the direct designs, however, are somewhat larger, the lowest cut-off frequency being significantly lower for the direct designs. Increasing the length of the filter improves accuracy significantly for time-delay designs, but only moderately for direct designs. It is also evident that H_1 is approximated well using relatively few terms, while the approximation of H_2 substantially poorer.

Overall, the filters designed using the time-delay approach are typically superior in performance, being more accurate for a given filter length and less sensitive to upstream

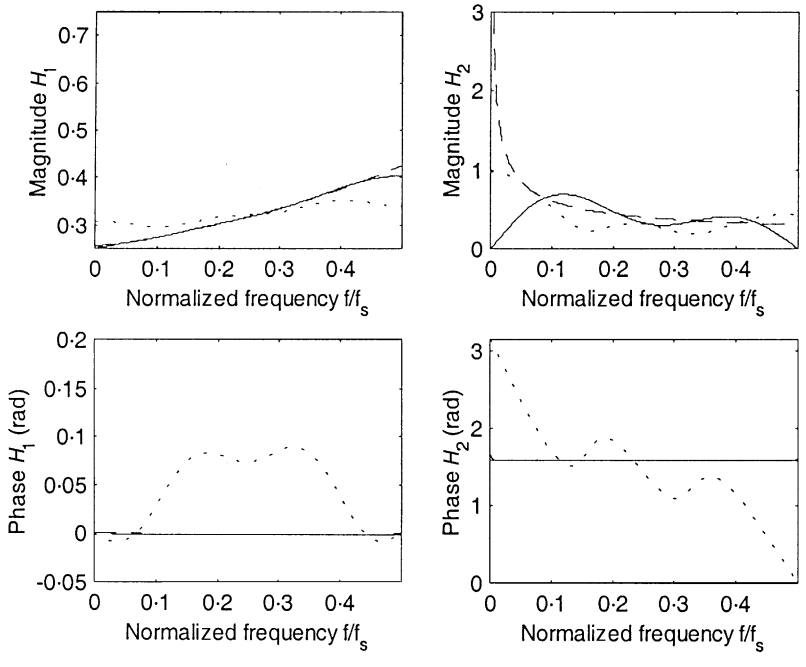

Figure 3. Frequency responses H_1 and H_2 of FIR filters, $n_t = 7$: ————, ideal; ————, time-delay design; ------, direct design.

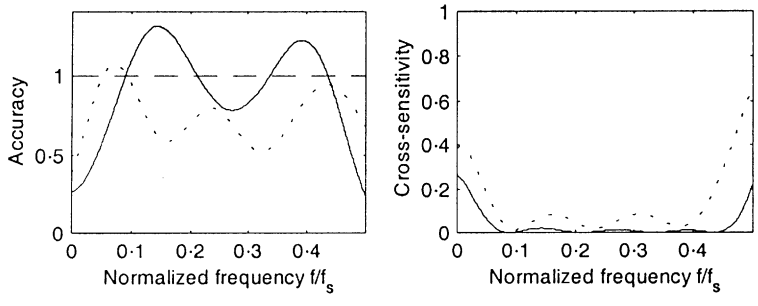

Figure 4. Accuracies and cross-sensitivities of FIR filters, $n_t = 7$: ————, ideal; ————, time-delay design; ------, direct design.

waves, Clearly, however, there must be a compromise between filter length (and hence accuracy and processing costs) and time delay.

4.4. GROUP DELAY, FILTER LENGTH AND ADAPTATION RATE

In addition to any time delay inherent in the filters, there is also a time delay that arises because of the time taken for a wave to propagate from the control location to the error sensor. This delay is

$$\tau = \frac{l}{c_g} = \frac{lk}{2\omega}, \tag{17}$$

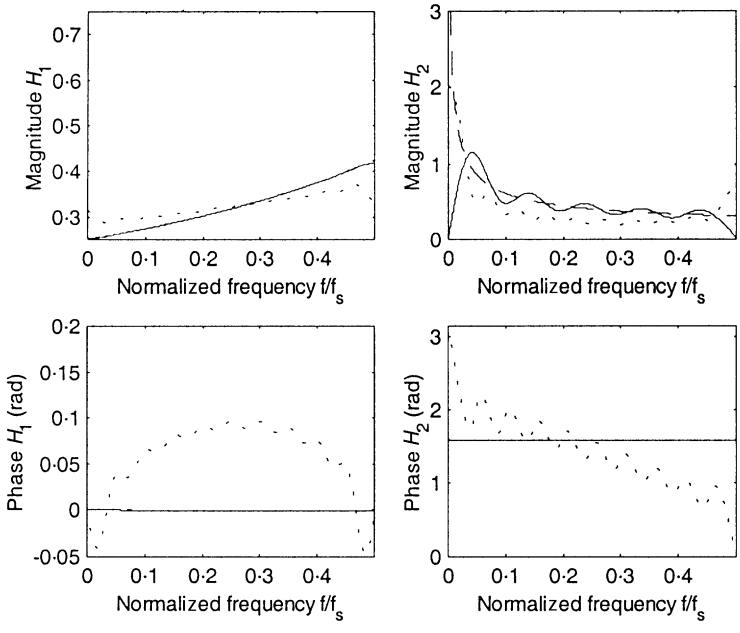

Figure 5. Frequency responses H_1 and H_2 of FIR filters, $n_t = 21$: ————, ideal; ————, time-delay design; ------, direct design.

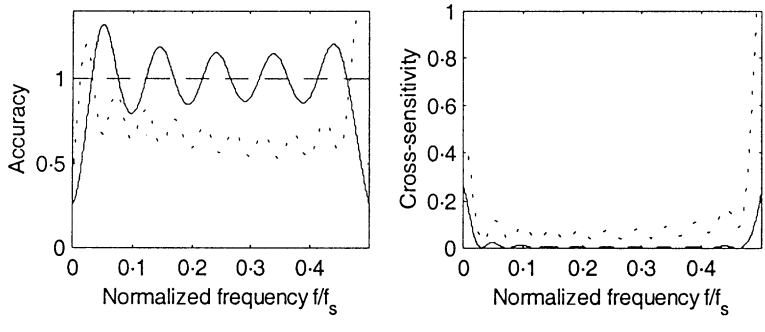

Figure 6. Accuracies and cross-sensitivities of FIR filters, $n_t = 21$: ————, ideal; ————, time-delay design; ------, direct design.

where c_g is the group velocity. This group delay is a maximum at the lowest frequency of interest, ω_{min}, and is approximately

$$\tau_{max} = \frac{l\sqrt{\pi}}{\lambda_n\sqrt{\omega_{min}}}. \tag{18}$$

For a typical array location, close to the control but outside its near field, this represents a delay of around five samples. This is in addition to any group delay of the filters.

The net effect of these time delays is that the maximum achievable adaptation rate is reduced [15, 16]. In effect, adaptation has to wait for the control input to pass through the

system and exit from the error sensor. In this respect, direct designs have an advantage. However, this may not be of great concern when using the filter output as a cost function for the adaptation. In practice, these time delays are likely to be small relative to that inherent in the filtered-X LMS algorithm. This is because the derivation of the algorithm is based upon the assumption of linearity and time-invariance, which is only a valid approximation if adaptation is slow [14]. The additional time delay in the filters is, therefore, unlikely to have a significant adverse effect on the adaptation rate.

In summary, the performance and the useful frequency range (between ω_{min} and ω_{max}) are limited by the following conflicting factors:

- the Nyquist frequency and the cut-off frequency of anti-aliasing filters affects ω_{max},
- the sensor spacing must be less than half a wavelength and affects ω_{max},
- the filter length n_t affects ω_{min}: the more terms in the filter, the lower ω_{min} is achievable,
- processing speed limitations may affect maximum filter length,
- the sensor array should ideally lie outside the near field of the control: this affects ω_{min},
- the distance of the sensor array from the control introduces a group delay,
- time-delay designs introduce additional group delays.

5. SIMULATIONS

5.1. PHYSICAL SYSTEM

The system being considered is shown in Figure 1. It is assumed that there are no reflections at end 1 (i.e., the end for which $x < x_s$) while reflections can occur from the end 2 at $x = x_2$. Of interest is the total vibration level in the region $x > x_c$, and the response is found at one or more points $x = x_r$, where x_r lies in some region between x_c and x_2. The effectiveness of the control is assessed in terms of the r.m.s. velocity at the response point before and after control. The "error sensor" is centered at $x = x_e$, and comprises two velocity sensors located at $x = x_e \pm \Delta/2$, which are therefore separated by a distance Δ. Their outputs are digitally filtered and combined to provide an estimate of the positive-going wave amplitude, as described in section 4. This single output is defined as the error signal.

It is assumed that the physical arrangement is similar to that shown in Figure 1, i.e., $x_1 \leqslant x_s \leqslant x_c < x_e \leqslant x_r < x_2$. Near fields are included in the simulations but ignored in the design of the error sensor filters so that ideally, the sensors should lie outside the near fields of the control force and the end at $x = x_2$.

5.2. SYSTEM DYNAMICS

5.2.1. *Sensor and actuator dynamics*

The disturbance and control actuators apply forces to the beam. It is assumed that the actuators have perfect dynamics, in that the force produced per unit input signal is a constant, independent of frequency. Similarly, the velocity sensors are assumed to have frequency-independent dynamics with constant unity gains.

5.2.2. *Beam response*

In the simulations, the end at $x = x_2$ is taken to have a matrix of reflection coefficients $\mathbf{r}_2$. This matrix relates the amplitudes of the reflected propagating and near field waves

$[\Phi_V^-(\omega)\ \Phi_{N,V}^-(\omega)]^T$ to those of the incident waves $[\Phi_V^+(\omega)\ \Phi_{N,V}^+(\omega)]^T$. It may take many values, for example,

$$\mathbf{r}_2 = \begin{bmatrix} 0 & 0 \\ 0 & 0 \end{bmatrix}; \qquad \mathbf{r}_2 = \begin{bmatrix} -1 & 0 \\ 0 & -1 \end{bmatrix}; \qquad \mathbf{r}_2 = \begin{bmatrix} -i & 1+i \\ 1-i & -i \end{bmatrix} \tag{19}$$

for an anechoic termination, for a simply supported end or for a free end respectively.

The frequency response of a thin beam is such that a time harmonic force $F\exp(i\omega t)$ injects velocity waves of amplitudes [2]

$$\Phi_V^+(\omega) = \Phi_V^-(\omega) = \frac{k}{\omega}\frac{F}{4\sigma},$$

$$\Phi_{N,V}^+(\omega) = \Phi_{N,V}^-(\omega) = -\,\mathrm{i}\frac{k}{\omega}\frac{F}{4\sigma}, \tag{20}$$

where Φ_V^+ and Φ_V^- are the amplitudes of the positive- and negative-going propagating waves at the excitation point, and $\Phi_{N,V}^+$ and $\Phi_{N,V}^-$ those of the near fields.

Suppose that a force is applied at some point. Waves leave the excitation point with amplitudes defined by equation (20). After they propagate over a distance x, the amplitudes become

$$\mathbf{H}_x(x;\omega) = \mathbf{fe}, \quad \mathbf{f} = \begin{bmatrix} \mathrm{e}^{-\mathrm{i}kx} & 0 \\ 0 & \mathrm{e}^{-kx} \end{bmatrix}, \quad \mathbf{e} = \frac{\beta}{\sqrt{\omega}}\begin{Bmatrix} 1 \\ -\mathrm{i} \end{Bmatrix}, \tag{21}$$

where $\mathbf{f}(x)$ is a propagation matrix, $\mathbf{e}$ the vector of injected wave amplitudes and β is a constant that depends on the excitation level and the beam properties. For convenience, it is assumed that $\beta = 1$ so that

$$\mathbf{H}_x(x;\omega) = \mathbf{fe}; \quad \mathbf{f} = \begin{bmatrix} \mathrm{e}^{-\mathrm{i}kx} & 0 \\ 0 & \mathrm{e}^{-kx} \end{bmatrix}; \quad \mathbf{e} = \frac{1}{\sqrt{\omega}}\begin{Bmatrix} 1 \\ -\mathrm{i} \end{Bmatrix}. \tag{22}$$

The velocity at x is given in terms of the velocity wave amplitudes by

$$v(x) = [1 \quad 1]\mathbf{H}_x. \tag{23}$$

In the real-time simulations impulse response functions, rather than frequency response functions, are required. In principle, this merely involves finding the inverse Fourier transform of $\mathbf{H}_x$. However, difficulties arise in practice for the following reasons. Firstly, $\mathbf{H}_x$ becomes infinite at $\omega = 0$ (i.e., a constant force produces constant acceleration and hence infinite velocity in the "steady state"). Secondly, in a digital implementation, problems arise for frequency components above the Nyquist frequency. If these higher frequencies are not removed, then their aliases contribute to $\mathbf{H}_x$. However, if they are neglected, then the resulting impulse responses are non-causal. Finally, if they are removed by filtering, then, in effect, $\mathbf{H}_x$ must be passed through a low-pass filter, so that the effective frequency response differs from $\mathbf{H}_x$ of equation (22). In the simulations, $\mathbf{H}_x$ is band-pass filtered in the range $(0{\cdot}05f_n$–$0{\cdot}95f_n)$ to remove the low- and high-frequency components.

5.2.3. *Propagation paths*

Six different impulse responses are required to describe wave propagation on the beam. The *primary paths* are the paths between the disturbance source input and the outputs of the

individual sensors in the error sensor array. The two relevant impulse responses are those that are between the disturbance force and the outputs of the two velocity sensors. The *cancellation paths* are the paths between the control force input and the outputs of the individual sensors in the error sensor array, the two relevant impulse responses being those between the control force and the outputs of the two velocity sensors. Finally, the *response paths* are the paths between the disturbance source and the control force inputs and the output of the response sensor.

The frequency responses of each of these paths have two components, namely a *direct component* and a *reflected component*, which is merely the reflection of the direct component from the end at $x = x_2$. For example, the impulse response relating the response sensor output to the control force input is found from the frequency response

$$H_{c,r}(\omega) = [1 \quad 1]\mathbf{f}(x_r - x_c; \omega)\mathbf{e} + [1 \quad 1]\mathbf{f}(x_2 - x_r; \omega)\mathbf{r}_2\,\mathbf{f}(x_2 - x_c; \omega)\mathbf{e}, \tag{24}$$

where the first term gives the direct component and the second term the reflected component.

All paths in the simulations are represented using FIR filters and the accuracy of the simulations is clearly dependent on these filters being of sufficient length.

5.3. CONTROL SYSTEM

Digital control is implemented, using FIR filters for all filtering operations. The control filter is adaptive, using a filtered-X LMS algorithm. In this, the updated filter weights are calculated from the expression

$$\mathbf{W}_{k+1} = \mathbf{W}_k + 2\mu e_k \mathbf{X}_k, \tag{25}$$

where $\mathbf{W}_k$ is the vector of filter weights, e_k is the error sensor output and $\mathbf{X}_k$ is the vector of inputs, with the subscript denoting the kth time step [14]. The constant μ is an adaptation

TABLE 1

Parameters used in simulation

Sample rate f_s	1024 Hz
Nyquist frequency $f_n = f_s/2$	512 Hz
Wavelength at Nyquist frequency	λ_n
Damping ε	0·001
Frequency range	0·05 f_n–0·95 f_n
Wave filter length n_t	11 terms ($n_d = 5$)
Cancellation path filter length	26 terms
Control filter length	64 terms
Adaptation parameter μ	0·0003
Sensor spacing Δ	0·3λ_n
x_s	0
x_c	2·1λ_n
x_e (farfield simulation)	3·6λ_n
(nearfield simulation)	2·7λ_n
x_r (farfield simulation)	5·1λ_n
(nearfield simulation)	4·7λ_n
x_2 (farfield simulation)	5·1λ_n
(nearfield simulation)	4·7λ_n

parameter that determines the speed and stability of adaptation, with too small a value resulting in slow adaptation, and too large a value resulting in poor attenuation or instability.

The parameters used in the simulations are given in Table 1. Controller parameters have been chosen to give moderately low order models that demonstrate the physical behaviour that is typically observed.

5.4. NUMERICAL EXAMPLES

Real-time simulations of wave-based adaptive control were performed using Matlab® and Simulink®. Anechoic and free terminations were simulated to illustrate the effects of reflections from the end. Simulations were also performed, using the velocity at the right-hand error sensor as the cost function, to compare the performance of the proposed wave-based approach with that of the conventional velocity-based control strategy.

Simulations were run for 100 s, with the average responses over a 20 s period from $t = 80$ s being found. In simulations of the anechoic termination, the response point was arbitrarily chosen at some distant downstream location, while for the free end simulations, the end of the beam was used as the response point. Simulations were performed with the error sensor array either distant from the control location or somewhat within the influence of its near field—these are referred to as "far field" and "near field" simulations in Table 1. The results of the simulations are shown in Figures 7–13. These figures show the r.m.s. response after control compared to that before control. Stated mean attenuations refer to the average attenuation attained over the frequency band $0{\cdot}1f_n$–$0{\cdot}9f_n$.

The performance of the wave-based control system when the error sensor is located outside the near field of the control actuator, for both anechoic and free end terminations, is

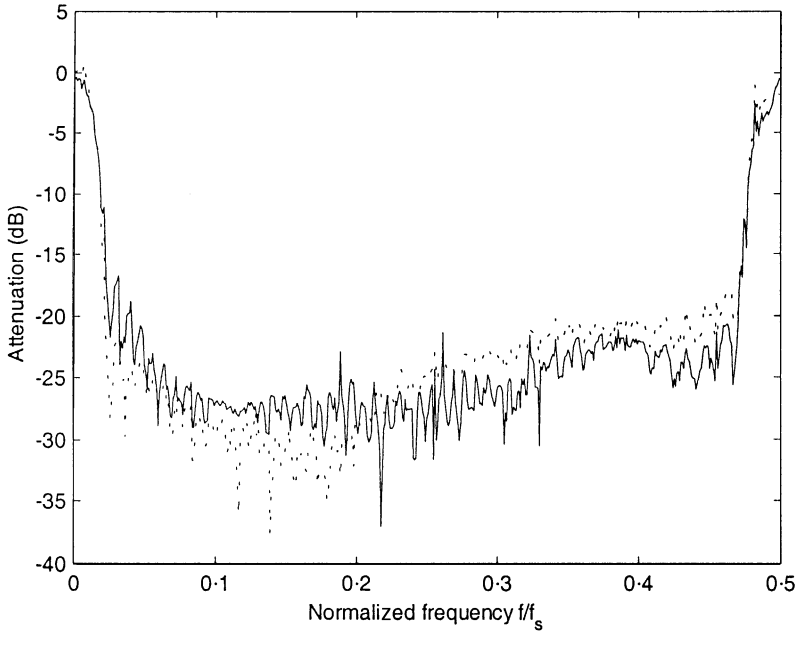

Figure 7. Attenuation under simulated wave-based control (error sensor in far field): ———, anechoic termination; - - - - - -, free end.

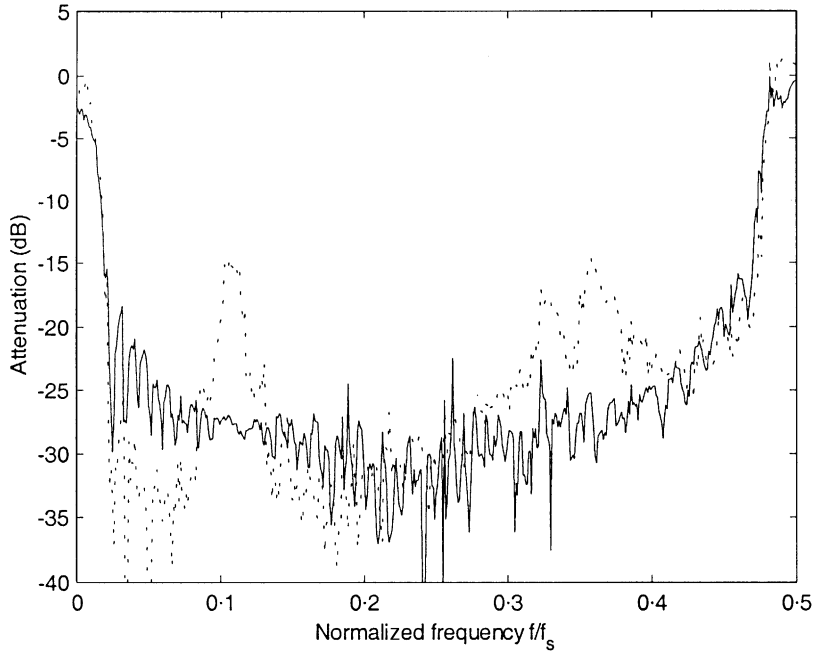

Figure 8. Attenuation under simulated velocity-based control (error sensor in far field): ———, anechoic termination; - - - - - -, free end.

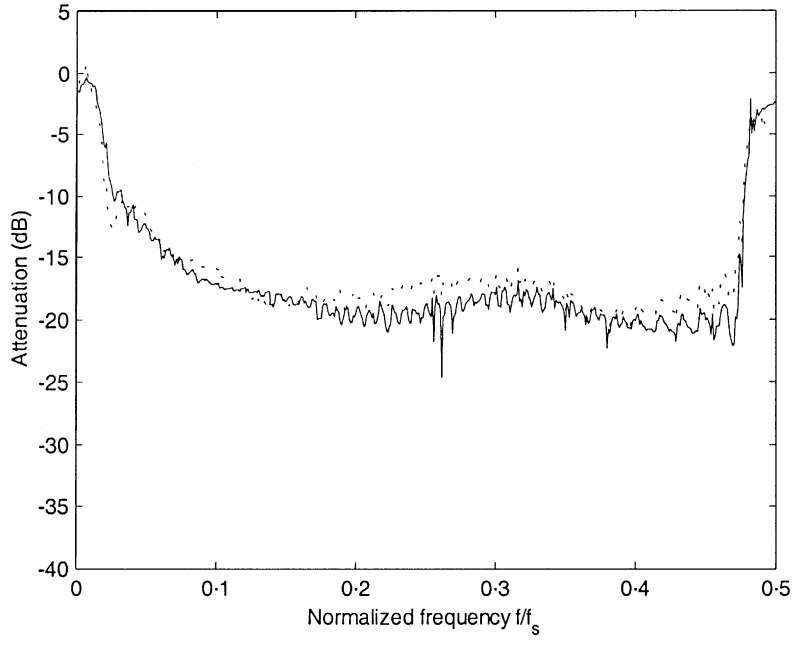

Figure 9. Attenuation under simulated wave-based control (error sensor in near field): ———, anechoic termination; - - - - - -, free end.

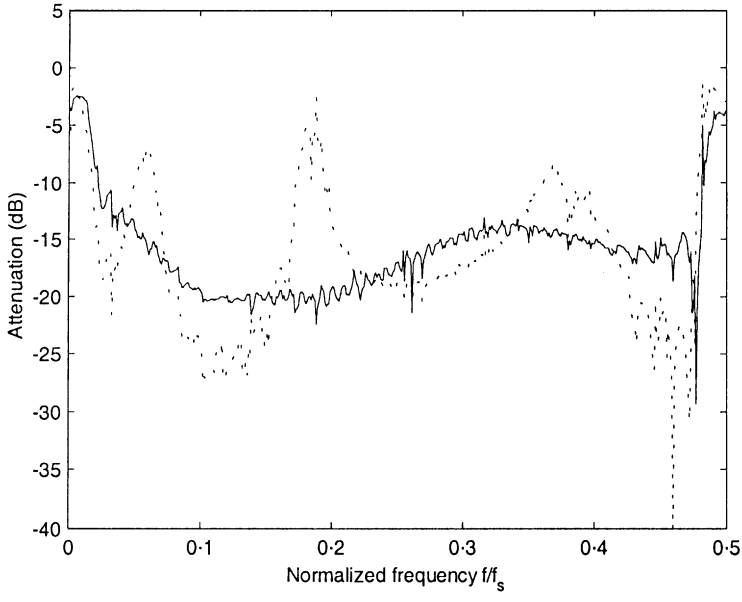

Figure 10. Attenuation under simulated velocity-based control (error sensor in near field): ———, anechoic termination; - - - - - -, free end.

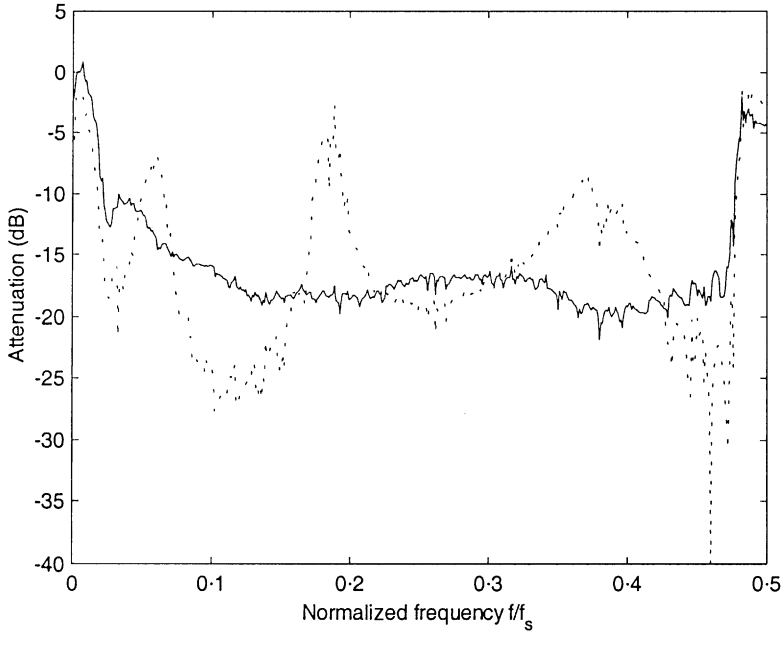

Figure 11. Simulated attenuation with free end termination (error sensor in near field): ———, wave-based control; - - - - - -, velocity-based control.

shown in Figure 7. It is apparent that the attenuation is largely independent of the end condition of the beam, with the anechoic termination resulting in a mean attenuation of 25·6 dB, compared to 24·7 dB for the free end. This is because the error sensor estimates the

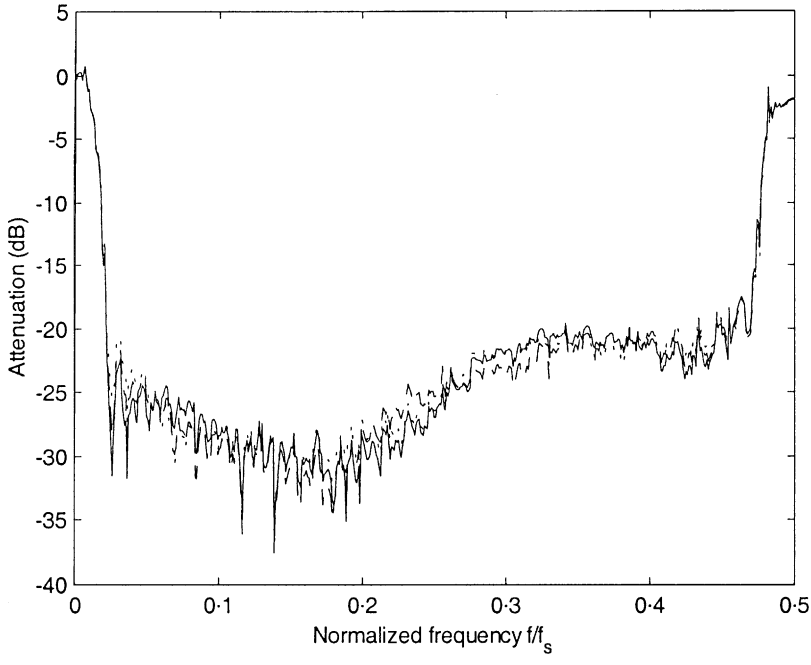

Figure 12. Simulated attenuation with free end termination (error sensor in far field): ——— 7, — — — — 11 and ------ 15 term wave filters.

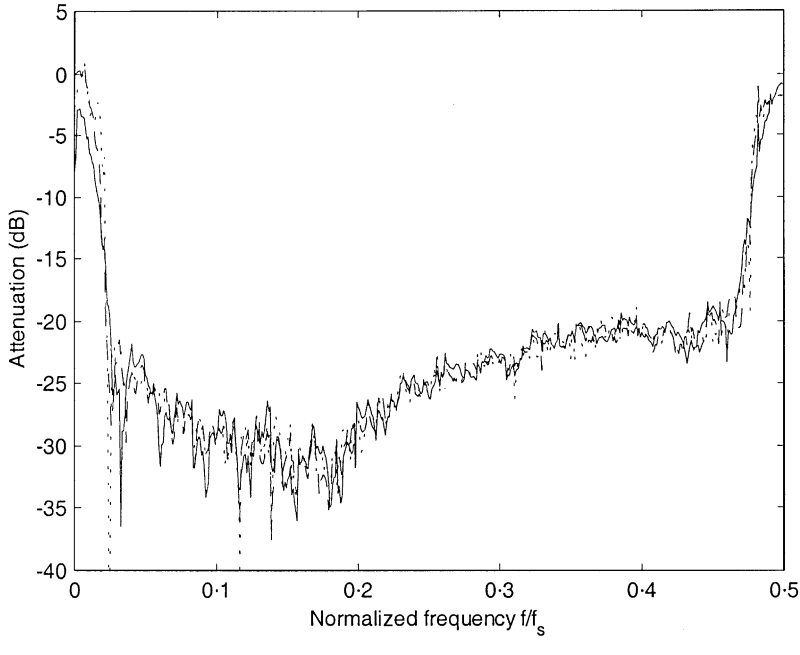

Figure 13. Simulated attenuation with free end termination (error sensor in far field): ——— 32, — — — — — 64 and ------ 128 term control filters.

downstream wave amplitude, which is independent of the end condition. Differences arise, for example, from imperfections in the filter design, which means that there is some cross-sensitivity to the upstream wave.

In Figure 8 is shown the performance of the velocity-based control system under the same circumstances. It can be seen that the levels of attenuation for the anechoic termination are similar to those achieved with wave-based control, with a mean attenuation of 27·7 dB. This is to be expected as there is no need for wave decomposition in the presence of a single propagating wave. The performance with the free end termination is significantly poorer in certain frequency bands, however, with a mean attenuation of 24·4 dB. This is because the reflective termination results in a standing wave between the control source and the free end. At those frequencies at which the error sensor is located close to a node of this standing wave (i.e., at $f/f_s \approx 0{\cdot}11, 0{\cdot}35$), any residual near field or noise strongly corrupts the error signal, and the resulting achievable control is small [15]. These effects become more apparent if the error sensor lies closer to the control actuator so that the near field of the control source is not extremely small. Figures 9 and 10 show the performance of the wave- and velocity-based control systems, respectively, under these circumstances. Comparing Figures 9 and 7, it is apparent that the presence of the near field has an adverse effect on the attenuation achieved by the wave-based control system, resulting in a mean attenuation of 18·5 dB. This is because the filters used in the error sensor were designed for farfield conditions, and the contribution of the near field is (wrongly) attributed to a propagating wave. Of more significance, however, is the fact that the control system performance is still largely independent of the beam termination, with the mean attenuation being 17·5 dB with the free end. The presence of a near field also reduces the performance of the velocity-based control system, resulting in a mean attenuation 16·9 dB with the anechoic termination. The influence of the beam termination is more significant than for the wave-based approach, however, as can be seen in Figure 10, with the mean attenuation being 15·2 dB for the free end. Figure 11 compares the performance of the two control systems with the free end termination. While velocity control gives somewhat better attenuation in certain frequency bands, wave control gives substantially better performance in others.

In summary, wave-based control offers superior broadband performance to velocity control primarily when there is a significant reflection from the downstream end.

Surprisingly, the performance of the wave-based control system is not strongly dependent on the length (and hence accuracy) of the filters used in estimating wave amplitudes. This is apparent in Figure 12, which shows the attenuation achieved with filters having 7, 11 and 15 terms.

In Figure 13 is shown the attenuation achieved with control filters having 32, 64 and 128 terms. These give very similar results, indicating that a 64-term filter is adequate for the simulations. Similarly, using cancellation path filters having lengths 16, 26 or 32 terms makes no discernible difference to the attenuation achieved.

A variety of values for the adaptation parameter, μ, were used. It is apparent from these simulations that the adaptation parameter can be substantially larger for wave-based control than for the velocity-based control, typically by a factor of 2 or more. This means that wave-based control can adapt more quickly and be more stable than the velocity-based control.

6. EXPERIMENTAL MEASUREMENTS

6.1. EXPERIMENTAL SET-UP

The experimental set-up comprised a steel beam having dimensions $6000 \times 50 \times 6$ mm suspended using piano wire at four points along its length. The "upstream" end of the beam was embedded in a sandbox to approximate an anechoic termination, while the

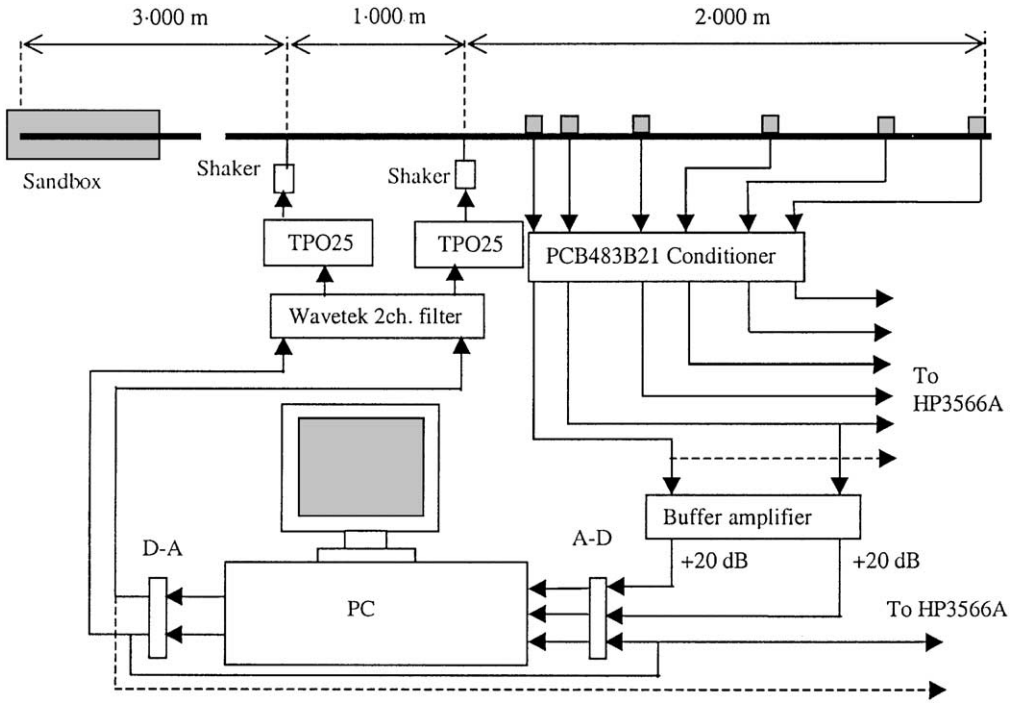

Figure 14. Experimental set-up.

"downstream" end of the beam was left free to ensure strong reflection of the incident propagating wave.

Excitation was supplied using a Ling V201 electrodynamic shaker, driving the centre of the beam through a stinger rod, while the control force was applied through an identical system located 1 m "downstream" of the disturbance actuator, as shown in Figure 14. The error sensor array comprised two PCB 353B65 piezoelectric accelerometers, separated by a distance of 70 mm $\approx 0{\cdot}3\lambda_n$. Two different error sensor array locations were used. In the first location, the centre of the array was 300 mm from the control actuator, ensuring that the influence of near fields on the sensor array was small. In the second location, the centre of the array was 135 mm from the control actuator. This resulted in a compact control system, but placed the error sensors so that the near field of the control actuator was of some significance. Four PCB 353B65 accelerometers were placed downstream of the error sensor array, as shown in Figure 14, to monitor the control system performance. The output of the sensor at the beam tip has been used in the presentation of the experimental results. In all the cases, the sensor outputs were integrated to give signals proportional to the velocity.

The disturbance and control signals were generated by a Pentium II® 350 MHz PC (incorporating 64 Mb of RAM), equipped with a Keithley Metrabyte® 1600 Series A–D/D–A board. All real-time processing was performed using Matlab® and Simulink® softwares, incorporating the Real-Time Workshop® and the Real-Time Windows Target®. The disturbance signal, the control signal and the response were also monitored using a Hewlett Packard HP® 3566A 8-channel analyser. Parameters used in the experimental measurements are given in Table 2.

TABLE 2

Parameters used in experimental measurements

Sample rate f_s	2048 Hz
Nyquist frequency f_n	1024 Hz
Wavenumber/freq relationship	$k = 0{\cdot}842\sqrt{f}$
Wavelength at Nyquist frequency λ_n	0·233 m
Frequency range	200–800 Hz ($\approx 0{\cdot}2f_n$–$0{\cdot}8f_n$)
Wave filter length n_t	11 terms ($n_d = 5$)
Cancellation path filter length	32 terms
Control filter length	64 terms
Adaptation parameter μ	0·005
Sensor spacing Δ	0·070 m ($\approx 0{\cdot}3\lambda_n$)
x_s	0
x_c	1 m ($\approx 4{\cdot}3\lambda_n$)
x_e (farfield)	1·3 m ($\approx 5{\cdot}6\lambda_n$)
(nearfield)	1·134 m ($\approx 4{\cdot}87\lambda_n$)
x_r	3 m ($\approx 12{\cdot}9\lambda_n$)
x_2	3 m
Reconstruction (anti-alias) filter cut off	900 Hz

6.2. EXPERIMENTAL PROCEDURE

Both the wave- and the velocity-based control systems were implemented on the beam. In each case, operation of the system consisted of the following steps:

1. identification of the cancellation path;
2. design of a filter to approximate the cancellation path;
3. control of vibration.

The main differences between the numerical and experimental implementations are that the actuator dynamics are fully included, that quantization errors are present due to A–D and D–A conversion and that there is some reflection from the "upstream" end of the beam because the sandbox does not provide a perfectly anechoic termination.

For both the cancellation path identification and the control implementation, the disturbance signal was generated using the Simulink® random number generator. This was output directly via a D–A converter for the cancellation path identification, while for the control implementation, it was digitally bandpass filtered (200–800 Hz) prior to D–A conversion. The resulting analogue signal was then low-pass filtered (900 Hz cut off, constant delay) to eliminate high-frequency components, amplified and used to drive the disturbance shaker. The unfiltered output was also input to one A–D channel as the reference signal.

6.3. EXPERIMENTAL RESULTS

In this section, the results of control using both wave- and velocity-based control systems are presented. Two specific cases are considered. In the first case, the error sensor array is sufficiently distant from the control actuator that the effects of near fields are negligible, while in the second, the error sensor array is placed within the near field of the control

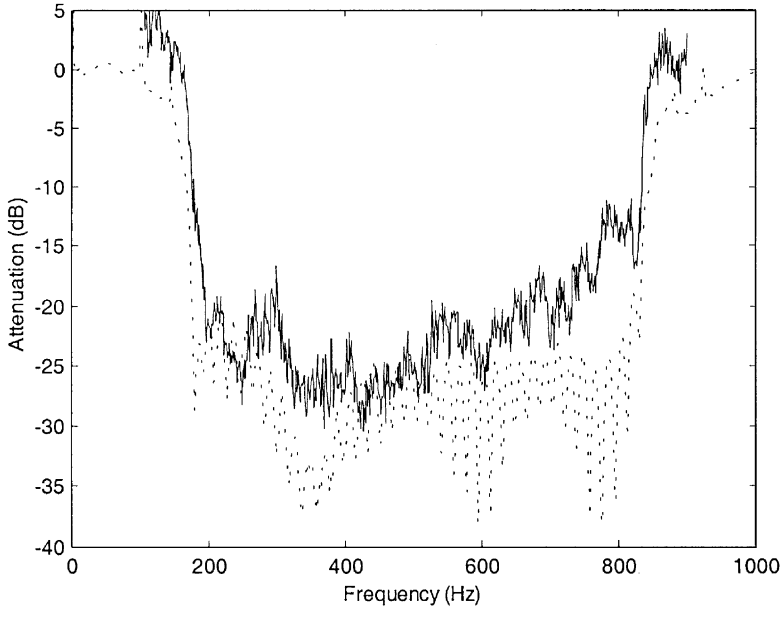

Figure 15. Attenuation with free end termination (wave-based control, error sensor in far field): ———, experiment; - - - - - -, simulation.

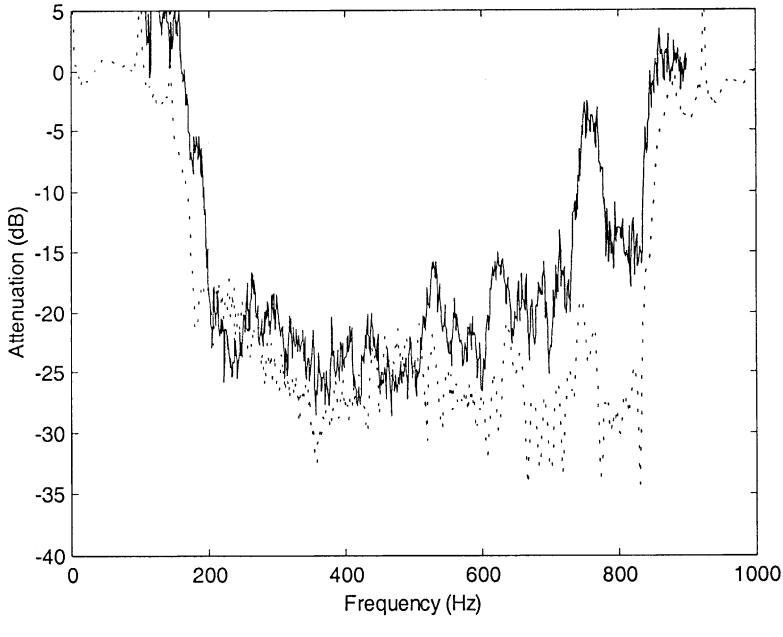

Figure 16. Attenuation with free end termination (velocity-based control, error sensor in far field): ———, experiment; - - - - - -, simulation.

actuator. The results are presented in terms of the r.m.s. velocity of the beam tip before and after control.

Figures 15–17 show the results obtained with the error sensor array located outside the near field of the control actuator. The results of wave-based control of the beam are shown

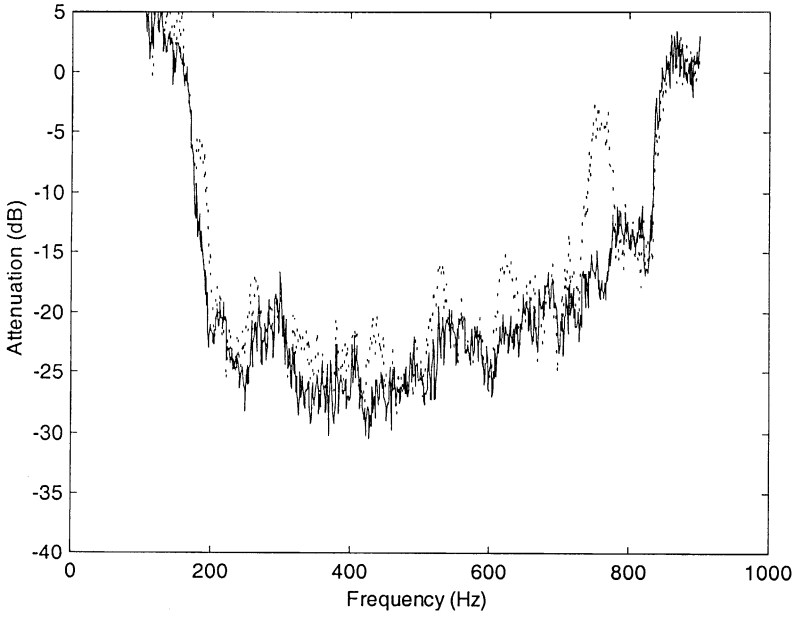

Figure 17. Measured attenuation with free end termination (error sensor in far field): ———, wave-based control; - - - - - -, velocity-based control.

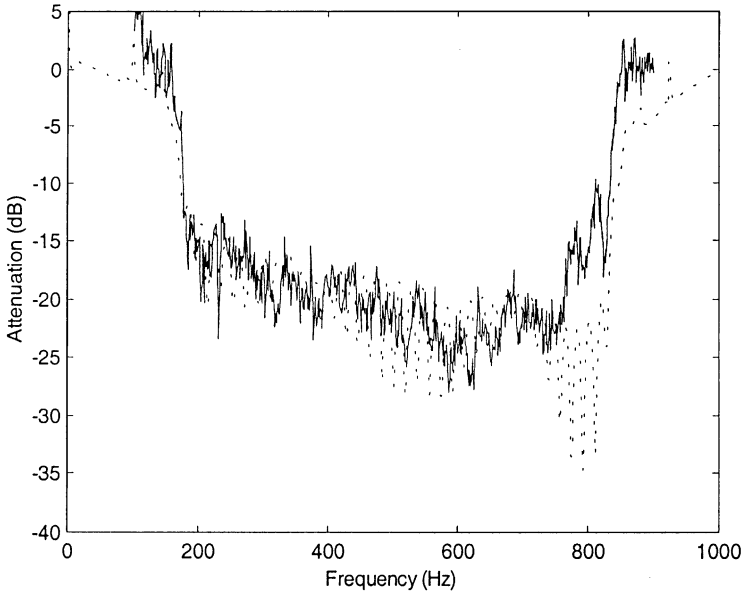

Figure 18. Attenuation with free end termination (wave-based control, error sensor in near field): ———, experiment; - - - - - -, simulation.

in Figure 15 and compared with simulations. It can be seen that the downstream response of the beam is reduced by typically 15–25 dB over the frequency range 200–800 Hz. In contrast, Figure 16 shows the results of velocity-based control of the beam, using the output of the right-hand (downstream) sensor as the cost function. It is apparent that the overall

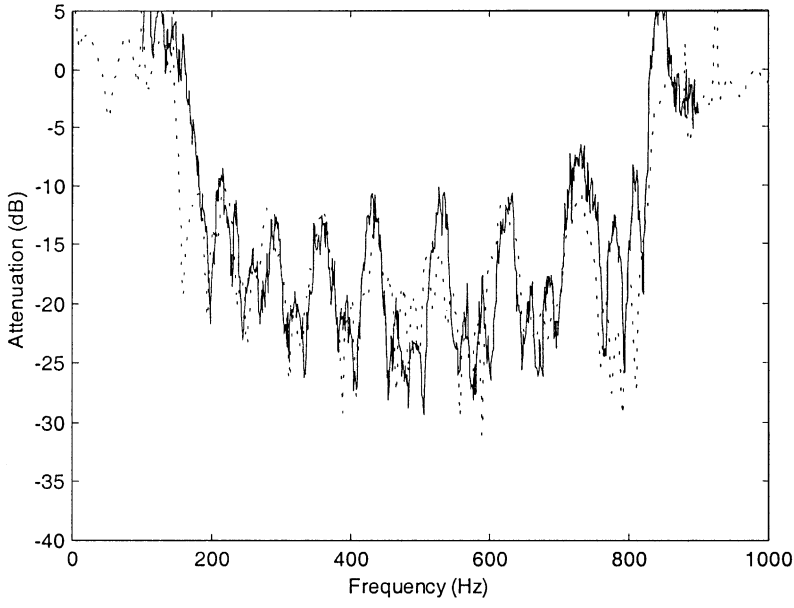

Figure 19. Attenuation with free end termination (velocity-based control, error sensor in near field): ———, experiment; - - - - - -, simulation.

attenuation is lower than that with wave-based control, with certain frequency bands exhibiting particularly poor attenuation. This is also evident in Figure 17, which shows the experimental results for the wave- and velocity-based controls.

Figures 18–20 show the results obtained with the error sensor array located within the near field of the control actuator. In Figure 18 are shown the results of the wave-based control, and it is apparent that the downstream response of the beam is reduced by typically 15–20 dB over the frequency range 200–800 Hz. In contrast, Figure 19 shows the results of the velocity-based control, using the output of the right-hand sensor as the cost function. It can be seen that the overall control performance is significantly poorer than that for the wave-based control, with distinct frequency bands of poor attenuation. These are also evident in Figure 20, which shows the experimental results for the wave- and velocity-based controls.

As discussed in section 5, the bands of poor attenuation under the velocity-based control are a consequence of the error sensor being close to a node of the standing wave, increasing the sensitivity to near fields and other sources of error. In the case of Figures 16 and 17, the influence of near fields on the error sensor is minimal, but the bands of poor attenuation are still evident. In the case of Figures 19 and 20, however, the error sensor is significantly influenced by the near field of the control actuator, and the resulting reduction in control system performance in distinct frequency bands is more readily apparent.

Experimental measurements also verified that the wave-based control system was relatively insensitive to changes in the length of the control, wave and cancellation path filters, as indicated by the simulations. However, it is apparent that there are significant differences between the simulations and the experimental measurements with the error sensor in the far field. In contrast, there is relatively good agreement between the simulations and measurements with the error sensor within the near field of the control actuator. This indicates that modelling discrepancies have a considerable effect on the

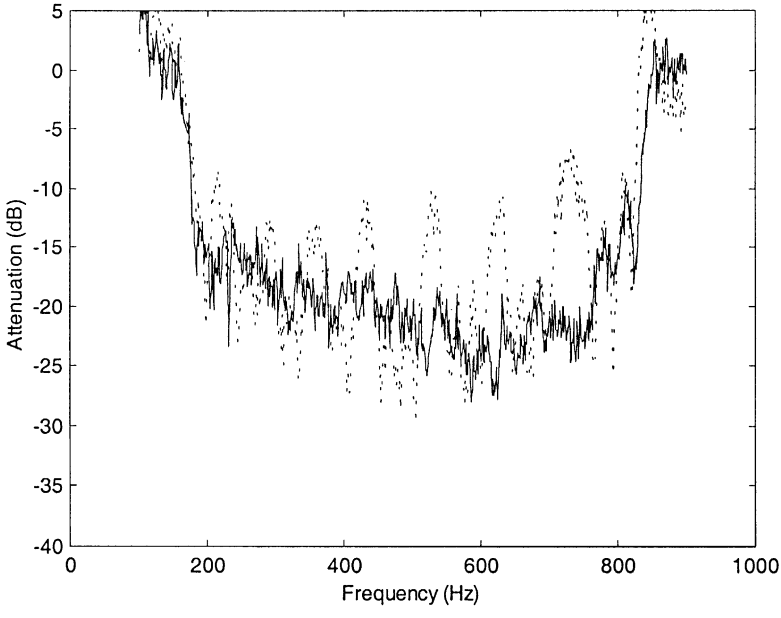

Figure 20. Measured attenuation with free end termination (error sensor in near field): ———, wave-based control; ------, velocity-based control.

control achieved in the former case, while they are not as significant in the latter case, where the dominant factor is the presence of the near field.

7. CONCLUDING REMARKS

The principles of a wave-based adaptive feedforward active vibration control system, using wave amplitude as a cost function, have been developed. The real-time estimation of propagating wave amplitude in the far field by combining and filtering the outputs of two velocity sensors has been described, and two approaches to the design of appropriate FIR filters have been proposed. Of these, the method based on a time delay appears to give the most promising results. Simulations show the proposed wave-based approach to have a performance similar to that of a conventional velocity-based system under anechoic conditions, but to offer significantly better broadband attenuation under reverberant conditions. Under these conditions, the velocity-based system can become very sensitive to the errors introduced by near fields and measurement noise. The wave-based system, being less sensitive to these factors, permits the error sensor to be placed closer to the control actuator, allowing the use of a more compact control system. Furthermore, the wave-based system appears to allow the use of a larger adaptation parameter, μ, thereby permitting faster adaptation or a greater margin of stability than is possible with the velocity-based approach. Altering the lengths of the control filter, the wave filters and the cancellation path filter were shown to have little effect on the control achieved, indicating that the lengths of these filters were adequate for the simulations. Experimental implementation of the control system on a steel beam showed good agreement between the simulations and experimental measurements.

ACKNOWLEDGMENTS

The authors gratefully acknowledge the financial assistance provided by the New Zealand Foundation for Research, Science and Technology, and the support of Industrial Research Ltd. in this work.

REFERENCES

1. S. J. ELLIOTT and L. BILLET 1993 *Journal of Sound and Vibration* **163**, 295–310. Adaptive control of flexural waves propagating in a beam.
2. B. R. MACE 1987 *Journal of Sound and Vibration* **114**, 253–270. Active control of flexural vibrations.
3. J. SCHEUREN 1990 *Proceedings of the Institute of Acoustics* **12**, 623–629. Active attenuation of bending waves in beams.
4. X. PAN and C. H. HANSEN 1993 *Journal of Sound and Vibration* **165**, 497–510. Effect of error sensor type and location on the active control of beam vibration.
5. A. E. SCHWENK, S. D. SOMMERFELDT and S. I. HAYEK 1994 *Journal of the Acoustical Society of America* **96**, 2826–2835. Adaptive control of structural intensity associated with bending waves in a beam.
6. A. H. VON FLOTOW and J. B. SCHAFER 1986 *Journal of Guidance and Control* **9**, 673–680. Wave absorbing controllers for a flexible beam.
7. N. TANAKA and Y. KIKUSHIMA 1999 *Journal of Vibrations and Acoustics* **121**, 174–182. Optimal vibration feedback control of an Euler–Bernoulli beam: towards realization of the active sink method.
8. P. AUDRAIN, P. MASSON and A. BERRY 2000 *Journal of the Acoustical Society of America* **108**, 612–623. Investigation of active structural intensity control in finite beams: theory and experiment.
9. C. H. HANSEN, A. J. YOUNG and X. PAN 1993 *Proceedings of the 2nd Conference on Recent Advances in Active Control of Sound and Vibration, Blacksburgh, VA*, 897–908. Active control of harmonic vibration in beams with arbitrary end conditions.
10. M. A. SWINBANKS 1973 *Journal of Sound and Vibration* **27**, 411–436. The active control of sound propagation in long ducts.
11. G. P. GIBBS, C. R. FULLER and R. J. SILCOX 1993 *Proceedings of the 2nd Conference on Recent Advances in Active Control of Sound and Vibration, Blacksburgh, VA*, 909–925. Active control of flexural and extensional power flow in beams using real time wave vector sensors.
12. A. C. ZANDER and C. H. HANSEN 1993 *Journal of the Acoustical Society of America* **94**, 841–848. A comparison of error sensor strategies for the active control of duct noise.
13. B. R. MACE and C. R. HALKYARD 2000 *Journal of Sound and Vibration* **230**, 561–589. Time domain estimation of response and intensity in beams using wave decomposition and reconstruction.
14. B. S. WIDROW and S. D. STEARNS 1985 *Adaptive Signal Processings*. Englewood Cliffs, NJ: Prentice-Hall.
15. C. H. HANSEN and S. D. SNYDER 1997 *Active Control of Noise and Vibration*. London: E & F N Spon.
16. X. PAN and C. H. HANSEN 1993 *Journal of Sound and Vibration* **168**, 429–448. Effect of end conditions on the active control of beam vibration.

APPENDIX A: NOMENCLATURE

c	wave velocity
EI	flexural stiffness
e	error signal, base of natural log
$\mathbf{e}$	vector of injected wave amplitudes
f	frequency
$h(t)$	impulse response

$H(\omega)$	frequency response
k	wavenumber
l	distance between control actuator and centre of sensor array
r	reflection coefficient (complex scalar)
$\mathbf{r}$	reflection coefficient (complex matrix)
R	reflection coefficient (magnitude)
$v(t)$	velocity (time domain)
$V(\omega)$	velocity (frequency domain)
x	location co-ordinate
$\mathbf{W}$	vector of filter weights
$\mathbf{X}$	vector of filter inputs
α	constant relating wavenumber to frequency
Δ	sensor spacing
ε	$-\mathrm{Im}(k)/\mathrm{Re}(k)$ (i.e., $k = \mathrm{Re}(k)(1 - \mathrm{i}\varepsilon)$)
ω	angular frequency
σ	beam mass per unit length
θ	phase
μ	adaptation parameter
τ	time delay
Φ	wave amplitude

Subscripts

C, c	control
e	error
g	group
k	kth time step
n	Nyquist frequency
N	near field
r	response
s	sampling rate or source
V	velocity
$+$, $-$	propagation/decay direction